

Production Strategy for Manufacturing Large-Scale AlSi10Mg Components by Laser Powder Bed Fusion

Original

Production Strategy for Manufacturing Large-Scale AlSi10Mg Components by Laser Powder Bed Fusion / Bosio, F., Shen, H., Liu, Y., Lombardi, M., Romestch, P., Wu, X., Zhu, Y., Hunag, A.. - In: JOM. - ISSN 1047-4838. - ELETTRONICO. - (2021). [10.1007/s11837-020-04523-8]

Availability:

This version is available at: 11583/2860604 since: 2021-01-12T12:26:23Z

Publisher:

Springer

Published

DOI:10.1007/s11837-020-04523-8

Terms of use:

This article is made available under terms and conditions as specified in the corresponding bibliographic description in the repository

Publisher copyright

Springer postprint/Author's Accepted Manuscript

This version of the article has been accepted for publication, after peer review (when applicable) and is subject to Springer Nature's AM terms of use, but is not the Version of Record and does not reflect post-acceptance improvements, or any corrections. The Version of Record is available online at: <http://dx.doi.org/10.1007/s11837-020-04523-8>

(Article begins on next page)

[Click here to view linked References](#)

Production Strategy for Manufacturing Large-scale AlSi10Mg Components by Laser Powder Bed Fusion

Federico Bosio^{a, b, c, 1}, Haopeng Shen^{a, b, 1}, Yang Liu^{a, b}, Mariangela Lombardi^c, Paul Rometsch^{a, b, 2},
Xinhua Wu^{a, b}, Yuman Zhu^{a, b, *}, Aijun Huang^{a, b, *}

^a Monash Centre for Additive Manufacturing, Notting Hill, VIC 3168, Australia

^b Department of Materials Science and Engineering, Monash University, Clayton, VIC 3800, Australia

^c Department of Applied Science and Technology, Politecnico di Torino, Corso Duca degli Abruzzi 24, 10129 Torino, Italy

Abstract

The long production time required for large-scale parts fabricated by laser powder bed fusion (LPBF) tends to induce cracks, distortions, and overheating problems. In this work, to address these challenges, we explore and establish a suitable strategy for producing large AlSi10Mg components. The platform temperatures preventing cracks and distortions are **firstly** determined. Then, the in-situ aging behavior is investigated for samples under various platform temperatures and holding times. **The rOur results** reveal that the platform temperatures of 150 °C and 200 °C **couldan** effectively prevent cracks and minimize distortions. **Also Besides**, using 150 °C, samples can reach the peak hardness with **the a** holding time less than 13 hours. In comparison, those samples produced with **a longer** holding time **longer** than 13 hours at 150 °C and 200 °C show obvious over-aging response and thus lower hardness. However, such a hardness **impoverishment** can be **recovered-improved mainly** by using a T6 post-process heat-treatment.

¹ These authors contribute equally to the work.

² Present address: Arvida Research and Development Centre, Rio Tinto, Jonquiere, QC G7S 4K8, Canada.

* Corresponding authors.

E-mail addresses: yuman.zhu@monash.edu (Y.M. Zhu), aijun.huang@monash.edu (A.J. Huang)

1. Introduction

Laser powder bed fusion (LPBF), as one of the typical additive manufacturing (AM) technologies, is a profitable alternative to conventional casting for the production of complex-shaped metal parts [1,2]. However, the former LPBF printing machines with limited building chamber dimensions only allow the fabrication of small-size components. Therefore, LPBF systems (the LPBF equipment) with higher building volumes has have been recently introduced to the market for large-scale manufacturing. Nevertheless, producing massive components pieces of aluminum alloys by LPBF still involves essential challenges to tackle solve till now. Notably, One issue is represented by the internal residual stresses arising from the rapid solidification. Such stresses associated with the LPBF will generate severe distortion and cracks, and will eventually lead to the job failure [3]. Since the LPBF process is relatively slow compared to foundry techniques, building large parts by LPBF requires relatively rather long printing time. Consequently, those defects must be prevented to the origin to save for saving time and powder. On this basis, heating the building platform throughout printing has been suggested to be effective in alleviating residual stresses and deformation of built parts [4]. Also, the heated building plate can reduce the solidification shrinkage of components due to the reduced thermal gradient [4,5].

Over the last decade, the Al-Si based alloys, i.e., 4xxx aluminum alloys, have been widely processed by LPBF with heated platform since their final products have high potentials to meet the industrial requirements in terms of for the lightweight, shape freedom and thermal conductivity [6–10]. Since these alloys are age-hardenable [11], the platform heating strategy can also induce the age-hardening effects to improve further the mechanical properties of the products besides in addition to alleviating distortions and cracks, which have been supported by several previous studies [12–14]. Specifically, Aversa et al. investigated the impact effect of various building platform temperatures on the strength and microstructure of an LPBFed A357 alloy [12]. Their results revealed the appearance of Mg₂Si precipitates at different building platform temperatures due to the in-situ aging induced by the heated platform during LPBF. Later, similar precipitates were confirmed by using differential scanning calorimetry (DSC) to examine the thermal ramp of an AlSi10Mg alloy processed by selective laser melting (SLM) with a platform heated ing at to 160 °C [13]. However, the hardness profile of a cylindrical bar with 100 mm in length did not show any significant age-hardening response along the building direction [13]. Recently, the precipitation of Si particles at a nano-scale has been reported in the as-built SLMed A357 alloy at with the platform temperature of 80 °C [14]. Also, satisfactory tensile properties have been reported, although the alloy exhibited a relatively low hardness in both as-built and directly aged conditions. The reason was mainly ascribed to the loss of solid-solution strengthening due to caused by the formation of nano-precipitates. Besides, a study demonstrated by Buchbinder et al. performed a systematic investigation on the effect of varied platform heating temperatures on distortions of AlSi10Mg components processed by SLM [15]. It was concluded that a platform temperature of 250 °C was appropriate to completely prevent distortions, although a low hardness value (~80 HV) was associated with the material. This value, however, is still higher than the hardness standard DIN EN 1706 for die-cast counterparts. Nonetheless, for the production of large-scale components, this hardness impoverishment could be further encouraged by the long holding time above with the heated platform and, therefore, more research is needed to solve this issue.

In this work, we propose a production strategy for manufacturing large parts of AlSi10Mg by LPBF is proposed. Two main fundamental vital design aspects are simultaneously concurrently addressed for the first time. The first is the prevention of cracks and support distortions, which that may lead to job failure. By using the platform heating strategy, we have first determined the platform temperatures that can alleviate macro-residual stresses by using an optimized processing setup. Then, the second crucial aspect addressed in this work is the age-hardening effect from induced by the heated platform. In this aspect, by producing the same samples with different printing times on a platform heated at 150 °C, we clearly show that the in-situ aging behavior not only depends on the holding time on the heated platform but also the position along the building direction. Also, the printing time limit to avoid in-situ over-aging at 150 °C is determined. Finally, for the production of

large-scale parts with a platform temperature of 200 °C, it is demonstrated that the over-aging occurs during printing, and a post-process heat treatment can effectively **recover** **increase** the hardness.

2. Materials and methods

2.1 Powder and LPBF process

Pre-alloyed gas-atomized powder of AlSi10Mg (TLS Technik GmbH & Co., Bitterfeld) was used in this work. The chemical composition of the powder can be found in supplementary Table **S1-I**. The direct current emission spectroscopy was used to detect metal elements (ASTM E 1097-12), while oxygen and nitrogen were analyzed via inert gas fusion (ASTM E 1019-11). The field-emission gun scanning electron microscope (SEM) JEOL JSM-7001F was used to evaluate particle shape and morphology. The size distribution was determined using laser diffraction analysis (Malvern Mastersizer 2000). Most particles of the gas-atomized powder have a spherical shape (Fig. 1a), and a mean size of 34 μm (Fig. 1b).

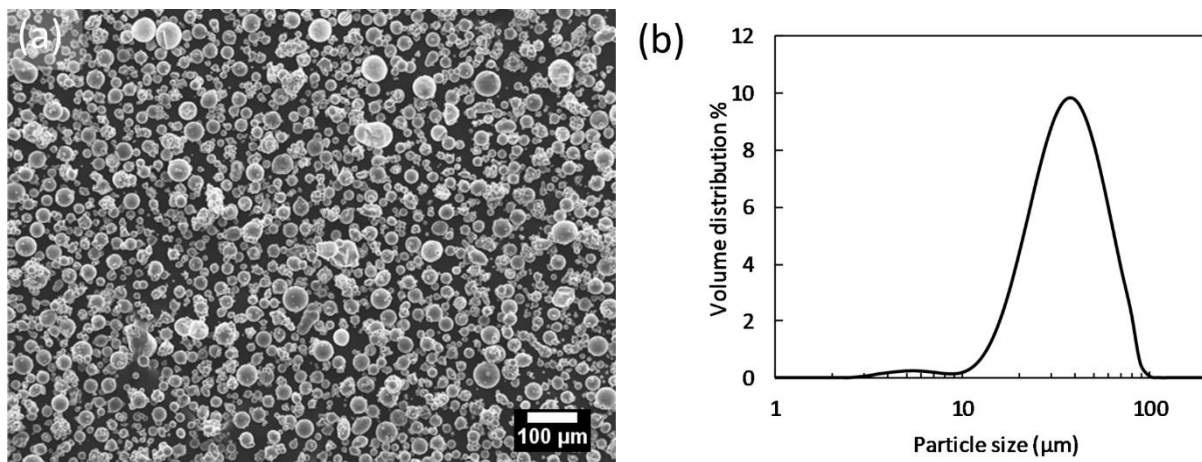


Fig. 1. (a) AlSi10Mg powder observed by SEM, and (b) powder size distribution.

The optimized processing parameters in an EOS M290 system (EOS GmbH) have been adopted in this work to **build** **manufacture** the AlSi10Mg specimens, see supplementary Table **S-II2**. A Yb-fiber laser with a wavelength of 1060-1100 nm and a nominal power of 370 W **was** **used** to melt a thin powder layer locally. The scanning speed of the laser was 1300 mm/s. Also, argon gas was applied in the building chamber to reduce the oxygen content below 0.1%. In addition, a 67° rotated scanning strategy was adopted to **have** **achieve** isotropic properties in the plane parallel to the building platform [16]. Heated building platform was utilized to investigate its effects on the cracks, distortions, and the in-situ aging response. It is worth noting that this strategy is different from the platform preheating for the LPBF [17,18]. We kept the platform at a constant temperature (T) throughout the building process. The specific T levels used in this study were selected based on the previous work, **see** **supplementary** **Table** **S2-II** [7,12–14].

2.2 Cracks and distortions assessment

The production of large parts can prematurely fail during LPBF when **the** internal residual stresses lead to severe distortions, cracks, delamination, and buckling. In this work, the platform heating method has been applied to alleviate these phenomena. To study the effect of various building platform temperatures on the formation of cracks and distortions, the ‘twin cantilever’ method proposed by Buchbinder et al. [15] was adopted **in** **for** this work. Cantilever samples with twin arms of 50 mm in length and 3 mm in thickness (Fig. 2) were built at T of 45 °C (RT), 100 °C, 150 °C and 200 °C. Surface profiles were recorded using a Mitutoyo CRYSTA-Apex S700 CNC coordinate measuring machine with a position accuracy of 1.7 μm to obtain the reference baseline. Then, support

pins of the right-hand arm were cut using electric discharging machining in the proximity of the building plate. All cantilever profiles were measured again to evaluate the extent of arm deflection after removal from the building plate. Profile measurements were carried out along the middle axis of the cantilever with a probe displacement of 1 mm. Five cantilever profiles for each condition were averaged to determine the overall deflection curve. On this basis, the appropriate platform heating temperatures were selected for the further in-situ aging study.

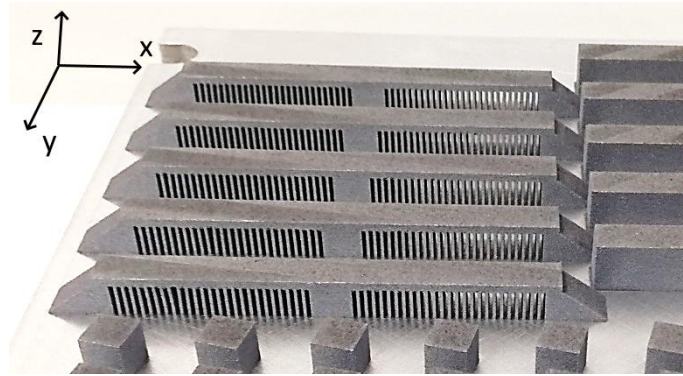


Fig. 2. Twin cantilever samples of AlSi10Mg alloy produced by LPBF. The z direction represents the building direction.

2.3 In-situ aging assessment

Building large parts by LPBF may require a long printing time (up to 1 week occasionally). The LPBF printing time, t , relies on the process parameters and volume number of parts to be printed. For this reason, two AlSi10Mg jobs with a low and high packing density of samples, corresponding to an LPBF printing time t of 13.4 hrs and 53 hrs respectively, were designed (Fig. 3). Parallelepiped samples with a dimension of $11 \times 85 \times 35 \text{ mm}^3$ were built by using a platform heating at for the platform temperature of $150 \text{ }^\circ\text{C}$. The Vickers micro-hardness (HV0.5) was evaluated along the building direction of as-built samples was evaluated using the Duramin A330 hardness tester with a load of 0.5 kg and a dwell time of 10 sec. Six samples for each condition were investigated to obtain the overall HV behavior. The hardness measurement was performed at specific height levels along Zz-axis. A total of 30 measures was made for each height level. The LPBF holding time of each height level can be determined by

$$\tau_i = \frac{(h - h_{i_HV})}{h} \cdot t \quad (1)$$

where τ_i is the LPBF holding time corresponding to the specific hardness tested level h_{i_HV} , h is the total sample height (35 mm), and t is the LPBF printing time.

Samples for SEM investigation were ground and polished, and then etched in Kroll's reagent for 15 sec. The SEM images and energy-dispersive x-ray spectroscopy (EDS) maps were obtained using the JEOL JSM-7001F microscope.

2.4 Post-process heat treatments

The Cubes with the a dimension of $10 \times 10 \times 10 \text{ mm}^3$ were produced using a platform heating temperature of $200 \text{ }^\circ\text{C}$ and a printing time of roughly 10 hrs. To mimic the heated platform effect for large parts, we have conducted a long-term isothermal heat treatment at $200 \text{ }^\circ\text{C}$ for up to 100 hrs on the as-built samples. The temperature inside the furnace chamber was set at the same T used throughout LPBF and monitored by a thermocouple ($\Delta T \pm 1 \text{ }^\circ\text{C}$). Later, all samples were heat-treated by a T6-like solution ($520 \text{ }^\circ\text{C}/1 \text{ h} + \text{water quenching} + 160 \text{ }^\circ\text{C}/6 \text{ h}$) to evaluate the effect of such heat treatment on the hardness and microstructure. The gap time between a solid solution and artificial

aging was controlled and kept below 30 min. For each sample, five Vickers hardness (HV 0.5 kg/10 see) measurements along the building direction were performed according to ASTM E92-17.

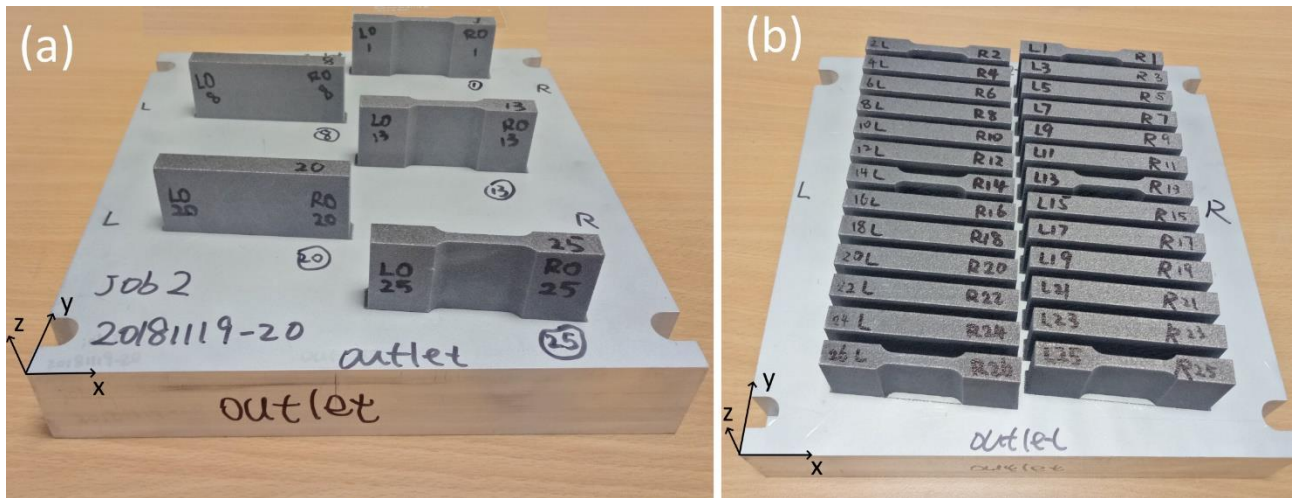


Fig. 3. (a) Low and (b) high packing density jobs of AlSi10Mg samples, corresponding to a total LPBF printing time of 13.4 hrs and 53 hrs, respectively. The z-direction represents the building direction.

3. Results

By using the platform heating strategy, the platform temperatures able to that can prevent cracks are first examined to uncover a safe route of for the production for of large-scale components (Fig. 4a-b). The micrographs in Fig. 4a depicts cantilever parts built at different platform heating temperatures T before the ahead of supports removal. A qualitative analysis of Fig. 4a these images reveals that various defects, such as cracks and support distortions, appear at 45 °C and 100 °C. The origin of these defects is associated with the first consolidated layers between the support structure and horizontal arms of twin cantilever samples. These distortions and cracks reduce significantly on the cantilevers built at 150 °C and 200 °C. The number of cantilever deflections as a function of the platform temperatures is shown in Fig. 4b. Given that most of the residual stresses generated in LPBF is are released after support removal, such stress they will give rise to the bent deflections associated with the samples. The maximum deflection ΔZ is recorded at the connection edge between the substrate and the cantilever built at 45 °C. For the At higher platform temperatures, the ΔZ reduction measured at cantilever edge is 34 % and 54 % for 100 °C and 150 °C, respectively. There is no obvious deflection detected at the platform temperature of 200 °C.

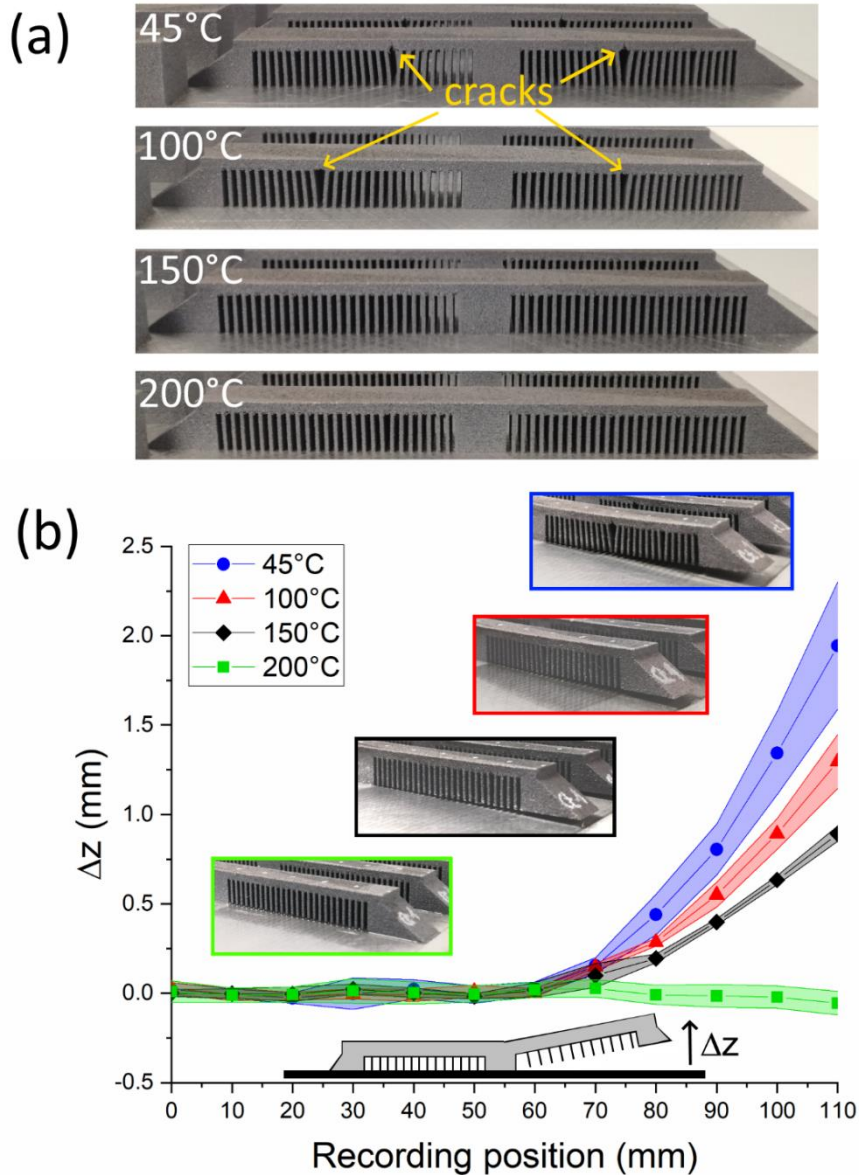


Fig. 4. (a) Macroscopic defects identified on twin cantilever samples at different platform heating temperatures; (b) Deflection (ΔZ) of twin cantilever after removing from the supports at different platform heating temperatures. Colored bands represent the measured standard deviations along the length of one side of the cantilever (from center to end). Inset pictures show the distortions at different plate temperatures.

Based on the results in Fig. 4a-b, the both platform temperatures of both at 150 °C and 200 °C can effectively prevent cracks formation and minimize distortions in cantilever parts, which is a vital requirement for a successful job when large LPBF parts are produced. Therefore, these two temperatures are selected for the subsequent in-situ aging studies. It should be noted that the former melted *i*-layer close to the heated substrate experiences a longer holding time than the later consolidated one (*i*+1 layer) during the LPBF process. Hence, the hardness associated with different sample height is also likewise different. Fig. 5 provides the hardness values along *ZZ*-direction of the samples with 35 mm in height that are built at a platform temperature of 150 °C for 13.4 hrs and 53 hrs. Considering the hardness profile after a printing time of 13.4 h, there is a significant hardness increment when the building time reached 2.5 hrs, which corresponds to the top part of the sample (i.e., *h* is between 23.7 and 35 mm). Then the hardness reaches a plateau value of ~137 HV between 2.5 hrs and 12.4 hrs. However, for the hardness profile after 53 h of printing time, a value drop in the curve can be identified after 53 hrs of printing time. This suggests suggesting the occurrence of over-aging in this part of the sample. Specifically, a peak-age of around 138.6 HV is firstly encountered at

τ of 13.4 hrs. Then, by further increasing τ , hardness is greatly reduced throughout the volume of material that experiences longer holding time, i.e., 49.2 hrs, on the heated platform. According to the results shown in Fig. 5, the AlSi10Mg building part has reached the peak-aged condition in most regions (up to $h = 27$ mm) with using a printing time of 13.4 hrs, whereas it is very probable that over-aging occurred when 53 hrs of LPBF printing time elapses.

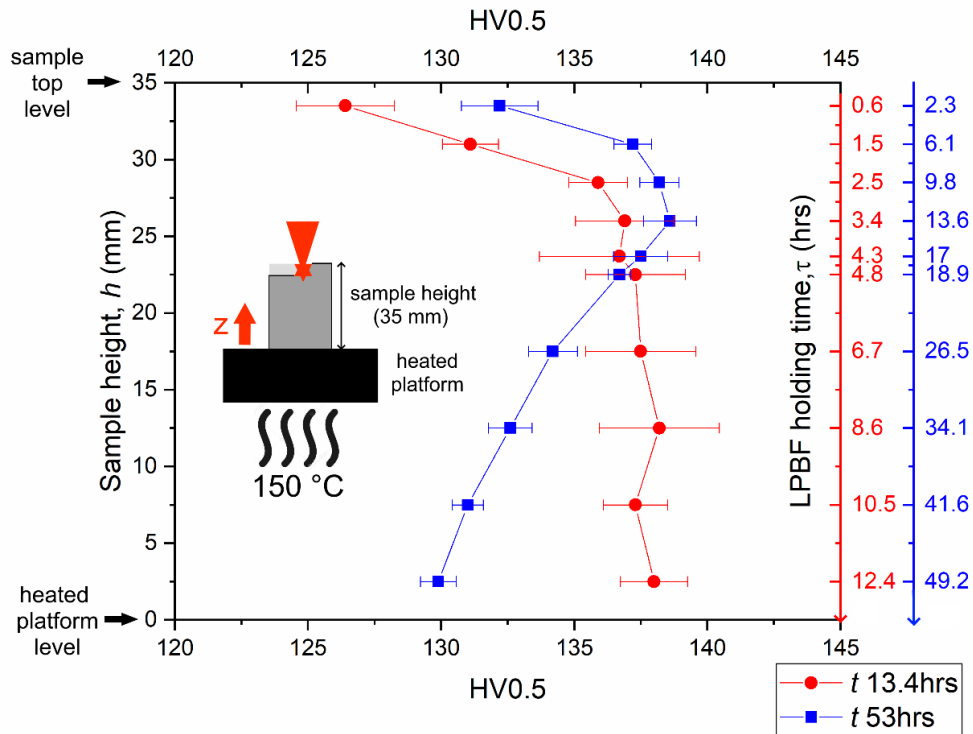


Fig. 5. Micro-hardness at different heights of AlSi10Mg samples built at different printing times (13.4 hrs and 53 hrs) at the platform temperature of 150 °C. The hardness values are plotted as a function of the specimen heights and the corresponding LPBF holding times.

Microstructural examination for selected positions of samples along the building direction further confirms the occurrence of in-situ aging, as shown in Fig. 6. Based on these images, the overall response of AlSi10Mg alloy to the fast cooling rate of LPBF process (1×10^5 K/s) [19] results in a very fine microstructure with submicron-sized primary α -Al cells (grey color) surrounded by fibrous eutectic boundaries (bright and light grey color). These eutectic boundaries are have been reported to be highly abundant in Si (see supplementary Fig. S-1), which is consistent with by previous studies on SLMed AlSi10Mg [20–22]. Since the investigated alloy is known to be sensitive to precipitation hardening, the presence of various intracolumnar super fine particles is remarkably higher when the samples experience longer holding times (Fig. 6e and 6f). There is no significant variation of α -Al column size in terms of dendrite width ($\lambda = 0.39$ – 0.44 μm). When the same sample height but different LPBF printing time are compared, a similar microstructural differences can be found, i.e. the higher number density of precipitates in Fig. 6d-f than in Fig. 6a-c.

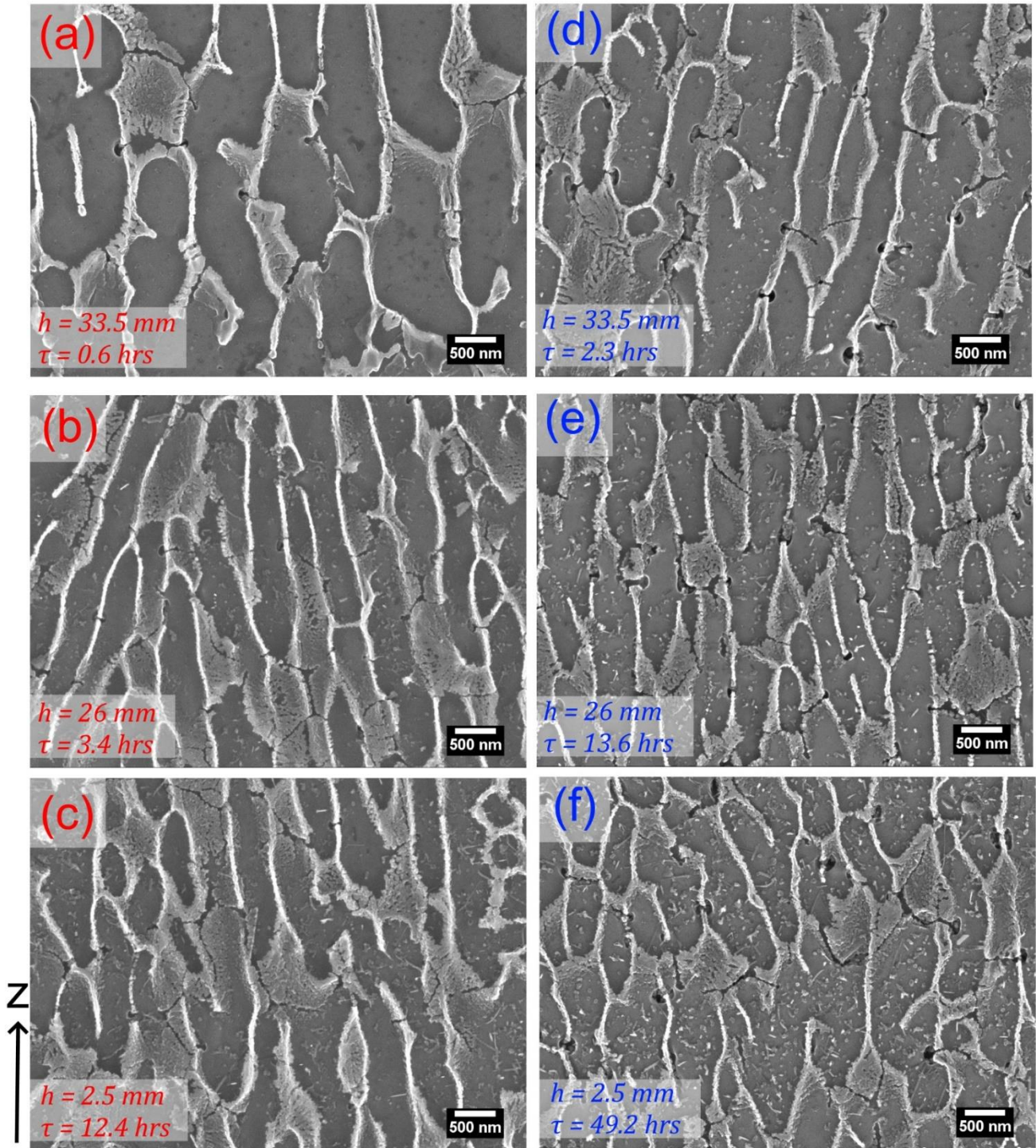


Fig. 6. Microstructure evolution along building direction of samples built upon (a-c) 13.4 hrs and (d-f) 53 hrs of printing time above a platform heated at 150 °C. Micrographs in (a-c) and (d-f) are arranged according to decreasing sample height (h) or increasing LPBF holding time (τ) (from top to bottom). SEM investigations were performed in a melt pool core next to the corresponding HV measurement reported in Fig. 5.

The hardness values of bulk AlSi10Mg samples processed with at the platform temperature of 200 °C and with an LPBF printing time of around-roughly 10 hrs are summarized in Fig. 7. As shown in the figure, two specific heat treatments have been designed. The former is a prolonged isothermal heat treatment at 200 °C to extend the heated platform effect for longer printing times (up to 100 hrs). The latter is the conventional T6-like heat treatment. Before the heat treatments, as-built samples show the hardness value of 100.5 ± 3 HV that is significantly far lower than those reported in the

literature [23,24]. Hence, it seems that AlSi10Mg samples are already overaged after 10 hrs of printing time at 200 °C. After an isothermal heat treatment at 200 °C for 100 hrs, a further decrease in hardness down to 91 ± 0.62 HV has been revealed. However, by applying a T6-like heat treatment on both conditions, the hardness values of 113.47 and 115.17 HV have been obtained. These values correspond to a hardness increase of 12% and 26 % for the as-built and isothermal heat-treated samples, respectively. Moreover, the hardness difference (around roughly 10 HV) between the as-built and isothermal heat-treated samples is offset by applying the T6 heat treatment. All the measured HV values lie in a narrow range between 111-118 HV, which is very close to the previously reported peak-aged hardness of the alloy after the T6 heat treatment [25,26].

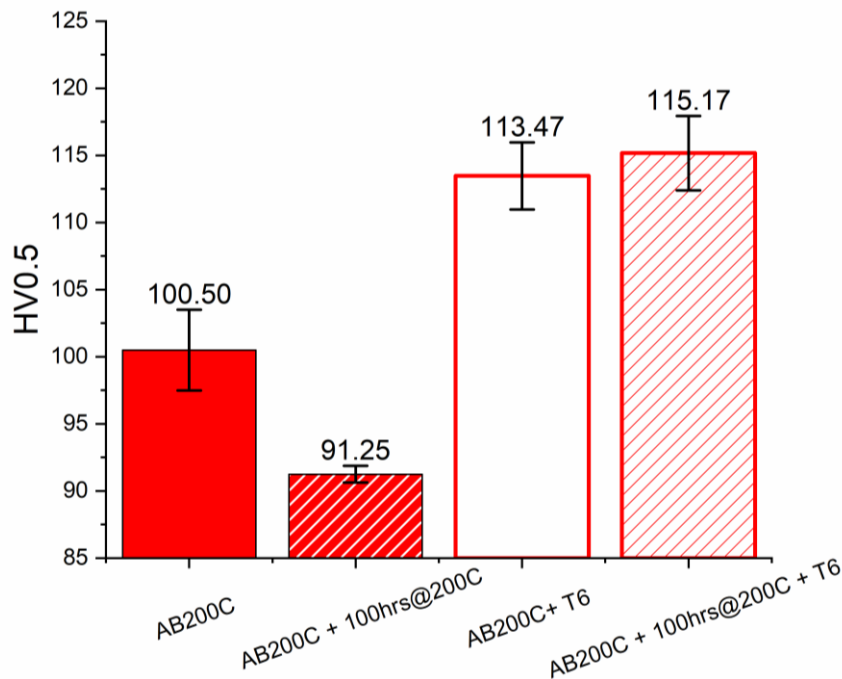
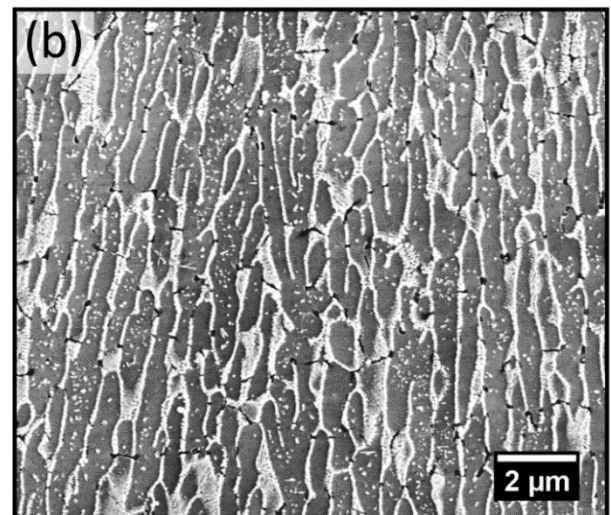
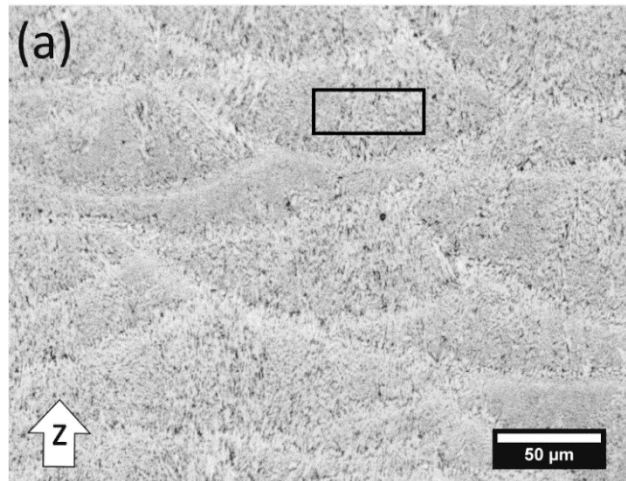


Fig. 7. Micro-hardness of the as-built and post-process heat-treated samples processed with a platform heating temperature of 200 °C.

The general microstructure of the as-built sample after isothermal heat treatment at 200 °C for 100 hrs is shown in Fig. 8a. The typical ‘fish scale’ pattern consists of dual-half elliptical melt pools aligned along the laser scanning direction. Fig. 8b provides a representative high-magnification micrograph taken from the core region of a melt pool. Here, the microstructure mainly includes submicron-sized primary α -Al cells surrounded by fibrous eutectic architecture. The observed morphology of α -Al is, to some extent, columnar rather than cellular because of the directional heat flux toward the building substrate. However, some rounded cells with a size of 0.41 ± 0.03 μm have also been identified. Moreover, a remarkable amount of tiny intracolumnar precipitates exist in the α -Al matrix. They are the most likely originated from the diffusion and precipitation of Si atoms.

Fig. 8c-d provide the representative micrographs of AlSi10Mg samples after the isothermal heat treatment and subsequent T6-like heat treatment. In Fig. 8c, the ‘fish-scale’ microstructure almost disappears because of the Al-Si eutectic and Si particles coarsening during the heat treatment. Note that few tracks of melt pool boundaries have been observed, as indicated by arrows in Fig. 8c. Inspection of the high-magnification image in Fig. 8d reveals the Si particles (light grey color see supplementary Fig. S-2) with the size range between 0.3 and 4 μm . Apart from these Si particles, some elongated precipitates with a plate-like shape have also been observed. They have a maximum length of 12 μm and averaged thickness of 0.41 ± 0.12 μm . These precipitates are likely the phase enriched in Fe, as evidenced by the EDS mapping shown in Fig. S-2. Such type of precipitates was also reported previously work in the SLMed A357 and AlSi10Mg after heat treatments [9,20].

AB200C + 100hrs@200C



AB200C + 100hrs@200C + T6

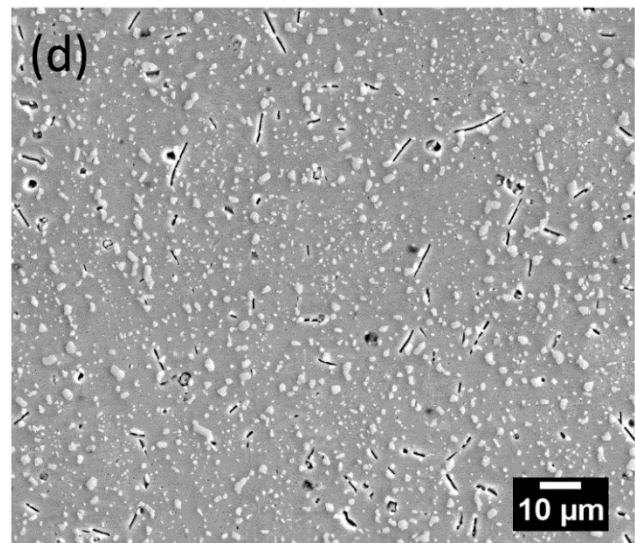
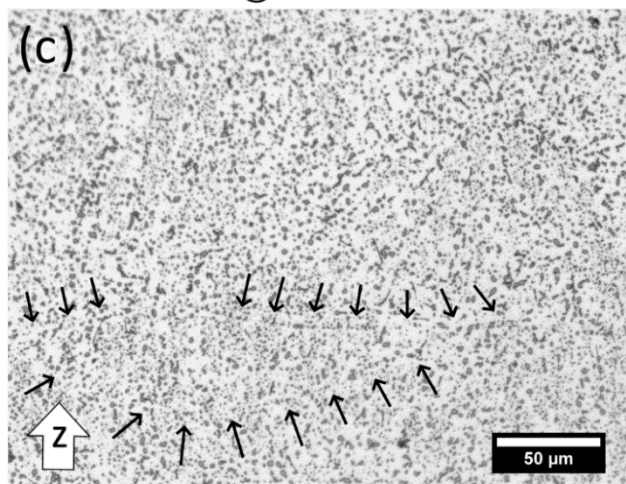


Fig. 8. (a) Optical and (b) SEM micrographs of AlSi10Mg sample after isothermal heat treatment at 200 °C for 100 hrs; (c) optical and (d) SEM micrographs of AlSi10Mg alloy after isothermal heat treatment (100 hrs at 200 °C) plus T6-like heat treatment.

4. Discussion

The production of massive AlSi10Mg parts ~~with critical shapes~~ involves essential challenges to deal with at the design stage due to the internal residual stresses ~~that~~ formed from ~~the~~ rapid cooling. As a result, preventing cracks and distortions has been the first key issue to be addressed. In this work, the building platform heating strategy has been adopted throughout the printing process to alleviate internal residual stresses. Four heating temperatures have been selected to find the proper ~~temperature level range~~ avoiding cracks and distortions. The results have revealed that ~~these~~ defects can be successfully prevented in cantilever samples ~~if~~ produced at a platform temperature of 150 °C and above. This ~~can be explained by the fact that is because~~ the solidification shrinkage of built parts can be reduced by the small temperature difference between the heated building platform and the AlSi10Mg solidus (557 °C) [27,28]. ~~In fact, w~~When the first powder layer of the cantilever arms is melted during LPBF, ~~in fact,~~ a natural thermal expansion of the melted alloy followed by a compression upon cooling is expected to occur. However, the shrinkage of the solidified layer is hindered by the robust support structure underneath, creating high tensile residual stresses in the opposite direction, which in turn will lead to fins bending and then crack initiation [15]. By increasing the platform heating temperatures, the current results have shown that cantilever deflections decrease at 150 °C and become negligible at 200 °C. The findings are in good agreement with the earlier research by Buchbinder et al. [15].

The Al-Si-Mg alloy is one of the main classes of heat-treatable alloys that exhibit apparent precipitation hardening response during aging [29]. Hence, it is technologically crucial to identify the in-situ aging effect for the long building time at upon the heated platform since such effect will eventually influence the mechanical properties of the parts. In this work, micro-hardness evaluation of parallelepiped samples processed on a platform heated up at 150 °C with different printing times has shown distinct aging behavior (Fig. 5). For the printing time of 13.4 hrs, the measured hardness along the building direction is consistent with the results of a heat treatable SLMed A357 alloy reported by Casati et al. [30]. It has to be noted that, in their work, a direct aging study was performed separately on bulk samples after the LPBF process, showing a peak-aged hardness of 137 HV for an aging time of 4 hrs at 160 °C. In comparison, the same hardness value has been achieved in the current work after around 3.4 hrs of holding time at a platform heating of 150 °C. As for the printing time of 53 hrs, our results have indicated the occurrence of the over-aging throughout the sample. A similar aging response was reported in a previous work [13] for a SLMed AlSi10Mg alloy directly aged in a furnace at 160 °C after printing on a non-heated platform. Also In addition, the over-aging can be evidenced by the microstructure examination shown in Fig. 6f. The evolution of microstructure immediately after melting involves the consolidation of the Si-supersaturated α -Al liquid primarily into a cellular/columnar structure with an extended Si solute content. Later, the residual Si segregates at the cell boundaries, generating a fibrous eutectic texture [21,31]. Due to the intimate contact with the heated platform, it was also highly probable that the high holding time experienced at 150 °C promotes the diffusion of the Si atoms in the α -Al supersaturated solid solution. In this way, a massive precipitation of fine intracolumnar particles takes place from accordingly, which disrupting the eutectic network and affecting the hardness. These fine particles were previously identified as pure Si particles in a SLMed A357 alloy with a direct aging at 160 °C for 8 hrs [9].

According to the current results, we advise adopting a platform temperature of 150 °C and holding times lower than 13 hrs to prevent the over-aging. Such a strategy will lead to more uniform hardness in the as-built sample and, simultaneously, partially release internal residual stresses without the need for post-process heat treatments. On the other hand, for large parts with critical shapes that require more than 13 hrs of LPBF printing, a platform temperature of 200 °C can be used to reduce internal stresses. However, a relatively low hardness value will be obtained, which is coupled with a microstructure severely enriched by sub-micron particles (Fig. 8b a). This weakening was presumably ascribed to the former Si diffusion from the α -Al supersaturated solid solution that contributed to the formation of fine precipitates within Si cells and the concurrent low-temperature stress relieving, as recently reported in Refs. [34,35] by Fiocchi et al. In this case, a remedy to the over-aging phenomena can be applied by using the post-process heat treatment [26,32,33]. When the T6 heat treatment was applied, the current work has witnessed a remarkable increase of hardness up to 115 HV, which is comparable to that of the die-cast A360-T6 counterparts [25,36]. Such a strengthening is mainly due to the dispersion of Si spheroids, which can act as obstacles to dislocation motion [33,37]. It is interesting to note that most published works have reported a slight impoverishment of strength in the heat-treated condition [9,25,33,37], which is different from the current results. Besides, the T6 heat treatment can also help to enhance fatigue properties of printed components, as documented by others [8,38]. Based on the above discussion, when LPBF processes large parts of aluminum, a new production strategy, including a platform heating of 200 °C and a T6-like heat treatment, can be applied to achieve in-situ stress relief and high hardness.

5. Conclusions

In summary, the present work has set up a production strategy for LPBF to produce large parts of AlSi10Mg by considering two main aspects: the inevitable presence of residual stress that can cause the job failure during long printing time, and the in-situ aging of the processed alloy. By using the platform heating strategy, we have first defined the platform temperatures for preventing cracks and support distortions. Then, these temperatures were adopted in the second stage for the in-situ aging investigations, leading to the following findings:

1. The building platform temperatures, setting at 150 °C and above, can effectively remove internal residual stresses and largely reduce part distortions for long-time LPBF jobs.
2. The in-situ aging response occurs at the platform heating temperature of 150 °C. The hardness reaches the peak with the holding time between 3.4 hrs and 13.4 hrs. The over-aging starts to appear when the holding time is longer than 13.4 hrs.
3. As-built and isothermal heat-treated samples processed at 200 °C clearly show the over-aging response, reaching the lowest HV value after 100 hrs at 200 °C.
4. The T6-like heat treatment was found able to recover the loss of hardness induced by the over-aging at 200 °C, increasing the HV value by 26 % in the best scenario.

In conclusion, for producing large parts with critical shapes, a platform heating temperature of 200 °C can be used to minimize distortions and bending of parts during LPBF. Nevertheless, the high printing time inevitably induces the over-aging weakening, and a the T6-like heat treatment can be applied to achieve mechanical properties comparable to the die-cast counterparts. On the other hand, for smaller parts requiring a printing time shorter than 13 hrs, a heated platform set at the aging temperature for Al alloys can be used to obtain directly peak-aged parts of AlSi10Mg without the need of any post-process heat treatments.

Acknowledgments

The authors acknowledge the financial support from the Australian Research Council, and the access to the facilities in the Monash Centre for Electron Microscopy (MCEM) and Monash Centre for Nanofabrication (MCN). The authors want to thank the experimental supports from Dr. Xiya Fang in the MCEM and Dr. Derui Jiang in the Monash Centre for Additive Manufacturing (MCAM).

References

1. D. Herzog, V. Seyda, E. Wycisk, and C. Emmelmann, *Acta Mater.* **117**, 371 (2016).
2. N. Li, S. Huang, G. Zhang, R. Qin, W. Liu, H. Xiong, G. Shi, and J. Blackburn, *J. Mater. Sci. Technol.* **35**, 242 (2018).
3. F. Calignano, *Mater. Des.* **64**, 203 (2014).
4. P. Mercelis and J. P. Kruth, *Rapid Prototyp. J.* **12**, 254 (2006).
5. M. F. Zaeh and G. Branner, *Prod. Eng.* **4**, 35 (2010).
6. T. Kimura and T. Nakamoto, *Mater. Des.* **89**, 1294 (2016).
7. H. Rao, S. Giet, K. Yang, X. Wu, and C. H. J. Davies, *Mater. Des.* **109**, 334 (2016).
8. E. Brandl, U. Heckenberger, V. Holzinger, and D. Buchbinder, *Mater. Des.* **34**, 159 (2012).
9. K. V. Yang, P. Rometsch, C. H. J. Davies, A. Huang, and X. Wu, *Mater. Des.* **154**, 275 (2018).
10. U. Tradowsky, J. White, R. M. Ward, N. Read, W. Reimers, and M. M. Attallah, *Mater. Des.* **105**, 212 (2016).
11. H. A. Ferguson, *Heat Treat. Alum. Alloy.* **4**, 841 (1991).
12. A. Aversa, M. Lorusso, F. Trevisan, E. Ambrosio, F. Calignano, D. Manfredi, S. Biamino, P. Fino, M. Lombardi, and M. Pavese, *Metals (Basel)*. **7**, 68 (2017).
13. M. Coduri, M. Hamidi Nasab, M. Vedani, R. Casati, and V. Tirelli, *Metals (Basel)*. **8**, 954 (2018).
14. J. H. Rao, Y. Zhang, K. Zhang, X. Wu, and A. Huang, *Mater. Des.* **182**, 108005 (2019).
15. D. Buchbinder, W. Meiners, N. Pirch, K. Wissenbach, and J. Schrage, *J. Laser Appl.* **26**, 012004 (2014).
16. F. Bosio, A. Aversa, M. Lorusso, S. Marola, D. Gianoglio, L. Battezzati, P. Fino, D. Manfredi, and M. Lombardi, *Mater. Des.* **181**, 107949 (2019).
17. A. H. Maamoun, Y. F. Xue, M. A. Elbestawi, and S. C. Veldhuis, *Materials (Basel)*. **12**, (2018).
18. A. H. Maamoun, Y. F. Xue, M. A. Elbestawi, and S. C. Veldhuis, *Materials (Basel)*. **11**, (2018).

19. T. DebRoy, H. L. Wei, J. S. Zuback, T. Mukherjee, J. W. Elmer, J. O. Milewski, A. M. Beese, A. Wilson-Heid, A. De, and W. Zhang, *Prog. Mater. Sci.* **92**, 112 (2018).
20. L. Zhou, A. Mehta, E. Schulz, B. McWilliams, K. Cho, and Y. Sohn, *Mater. Charact.* **143**, 5 (2018).
21. L. Thijs, K. Kempen, J. P. Kruth, and J. Van Humbeeck, *Acta Mater.* **61**, 1809 (2013).
22. S. Marola, D. Manfredi, G. Fiore, M. G. Poletti, M. Lombardi, P. Fino, and L. Battezzati, *J. Alloys Compd.* **742**, 271 (2018).
23. N. T. Aboulkhair, M. Simonelli, L. Parry, I. Ashcroft, C. Tuck, and R. Hague, *Prog. Mater. Sci.* **106**, 100578 (2019).
24. S. Marola, D. Gianoglio, F. Bosio, A. Aversa, M. Lorusso, D. Manfredi, M. Lombardi, and L. Battezzati, *J. Alloys Compd.* **821**, 153538 (2020).
25. L. Girelli, M. Tocci, M. Gelfi, and A. Pola, *Mater. Sci. Eng. A* **739**, 317 (2019).
26. A. H. Maamoun, M. Elbestawi, G. K. Dosbaeva, and S. C. Veldhuis, *Addit. Manuf.* **21**, 234 (2018).
27. P. Mercelis and J. P. Kruth, *Rapid Prototyp. J.* **12**, 254 (2006).
28. J. P. Kruth, J. Deckers, E. Yasa, and R. Wauthlé, *Proc. Inst. Mech. Eng. Part B J. Eng. Manuf.* **226**, 980 (2012).
29. C. H. J. Davies, K. Zhang, J. H. Rao, X. Wu, A. Huang, and Y. Zhang, *Scr. Mater.* **160**, 66 (2018).
30. R. Casati and M. Vedani, *Adv. Eng. Mater.* **1800406**, 1800406 (2018).
31. K. G. Prashanth, S. Scudino, H. J. Klauss, K. B. Surreddi, L. Löber, Z. Wang, A. K. Chaubey, U. Kühn, and J. Eckert, *Mater. Sci. Eng. A* **590**, 153 (2014).
32. S. Li, J. Liu, Y. Shi, Q. Wei, W. Li, A. Zhang, C. Yan, and Y. Zhou, *Mater. Sci. Eng. A* **663**, 116 (2016).
33. N. T. Aboulkhair, I. Maskery, C. Tuck, I. Ashcroft, and N. M. Everitt, *Mater. Sci. Eng. A* **667**, 139 (2016).
34. J. Fiocchi, A. Tuissi, P. Bassani, and C. A. Biffi, *J. Alloys Compd.* **695**, 3402 (2017).
35. J. Fiocchi and C. A. Biffi, *JOM* (2020).
36. L. Roger, *CSIRO Light Met. Flagsh.* (2008).
37. N. T. Aboulkhair, C. Tuck, I. A. N. Ashcroft, I. A. N. Maskery, and N. M. Everitt, *Metall. Mater. Trans. A* **46**, 3337 (2015).
38. N. T. Aboulkhair, I. Maskery, C. Tuck, I. Ashcroft, and N. M. Everitt, *JMADE* **104**, 174 (2016).